PCCP

Accepted Manuscript

ROYAL SOCIETY OF CHEMISTRY

www.rsc.org/pccp

PCCP

RSCPublishing

PAPER

NANOGOLD decorated by pHLIP Peptide: Comparative Force Field Study

Cite this: DOI: 10.1039/x0xx00000x

A. Kyrychenko*

Received 00th January 2012,
Accepted 00th January 2012

DOI: 10.1039/x0xx00000x

www.rsc.org/

The potential of gold nanoparticles (AuNPs) in therapeutic and diagnostic cancer applications is becoming increasingly recognized, focusing on their efficient and specific delivery from passive accumulation in tumour tissue to directly targeting tumor-specific biomarkers. AuNPs functionalized by *pH L*ow *I*nsertion *P*eptide (pHLIP), have recently revealed the capability to targeting acidic tissues and inserting into cell membranes. However, the structure of AuNP-pHLIP conjugates and fundamental gold-peptide interactions still remain unknown. In this work, we have developed a series of molecular dynamics (MD) models reproducing a small gold nanoparticle coupled to pHLIP peptide. We focus on Au_{135} nanoparticles that comprise a nearly spherical Au core (diameter ~1.4 nm) functionalized with a monomaleimide moiety, mimicking commercially available a monomaleimido NANOGOLD® labelling agent. To probe the structure and folding of pHLIP, attached covalently to the maleimide NANOGOLD particle, we have benchmarked the performance of a series of popular, all-atom force fields (FF), including those of OPLS-AA, AMBER03, three variations of CHARMM FFs, as well as united-atom GROMOS G53A6 FF. We found that CHARMMs and OPLSAA FFs predict that, in aqueous salt solution at neutral pH, pHLIP is partially bound onto the gold surface thought some short hydrophobic peptide stretches, while, at the same time, a large portion of peptide remain in solution. In contrast, AMBER03 and G53A6 FFs revealed the formation of compact, tightly bound peptide configurations adsorbed onto the nanoparticle core. To reproduce the experimental physical picture of the peptide adsorption onto gold in unfolded and unstructured conformations our work suggests CHARMM36, and OPLS-AA FFs as a tool of choice for computational studies of NANOGOLD decorated by pHLIP peptide.

1. Introduction

Over the past decades gold nanoparticle (AuNPs) have received extensive attention in cancer therapy as imaging and contrast agents for *in vitro* and *in vivo* near-infrared (NIR) laser photothermal treatments.[1] AuNPs can be easily prepared in a variety of shapes and sizes, and possesses easily controllable surface chemistry allowing functionalization with various biologically useful molecules, such as organic ligands and peptides, which help improving of their chemical functionality and tumour-targeting delivery. The unique photophysical properties of gold nanostructures have been utilized to enhance a number of spectroscopically relevant applications in biodiag–nostics and treatment monitoring, such as surface enhanced Raman scattering, metal enhanced fluorescence, and luminescence imaging.[2, 3] Targeted delivery of AuNPs to tumor tissue can be accomplished in a variety of ways, ranging from direct injection of bare AuNPs, followed by their passive accumulation, up to the use of AuNPs functionalized with targeting ligands, such as peptides and antibodies.[4,5]

Recently, a new strategy for targeting of acidic tissue *in vivo* has been suggested based on a 35-amino acid peptide derived from the bacteriorhodopsin C helix, which revealed the pH-selective insertion and folding in lipid membranes.[6] This peptide, called *pH* (*L*ow) *I*nsertion *P*eptide (pHLIP), was capable of active and rapid insertion into a lipid membrane and translocation of its C-terminal tail into cells.[7] These events occur by the formation of a rigid α-helix upon change of pH from 7.4 to 6.5, providing a novel platform for development of

*Institute of Chemistry and School of Chemistry, V. N. Karazin Kharkiv National University, 4 Svobody square, Kharkiv 61022, Ukraine
E-mail: a.v.kyrychenko@karazin.ua

† Electronic Supplementary Information (ESI) available: Figures S1-S5 and Table S1-S2. Examples of FF topologies of gold-maleimido-pHLIP in the GROMACS format, as well as coordinate files of AuNP-pHLIP in the GRO and PDB file formats. See DOI: 10.1039/b000000x/

drug-delivery systems.[8] A pH-driven targeting and translocating AuNPs is achieved by attaching pHLIP, which is constructed by conjugating a cysteine residue in its N-terminus.[2, 9-12] In most pHLIP's, the peptide inserts in a lipid membrane uni-directionally, so that it's C-terminus propagates across the bilayer and comes out inside the membrane. Therefore, a cargo molecule, such as a fluorescent imaging agent or a metal nanoparticle, attached to the pHLIP's N-terminus remains on the membrane surface and do not penetrate deeper in membrane after pHLIP insertion.[13] pHLIP derivatives have also been used for design of nanoparticle-based drug-delivery systems owing to their improved pharmacokinetics and pharmaco dynamics arising from the enhanced permeation and retention effect.[2, 9, 14-16,17] In spite of a fact that many biochemical applications based on gold nanoconjugates have shown a promising potential in anticancer treatment, the fundamental interactions and mechanisms of cell delivery to living systems for the most part still remain unknown.

In recent time, more attention has been directed toward theoretical understanding of molecular aspects governing specific, regioselective surface adsorption of peptides and polymers onto inorganic metal nanocrystals. Numerous molecular dynamics (MD) simulation studies of metal nanoparticles protected by organic ligand monolayer,[18-22] polymers,[23,24] and dendrimers[25] have been conducted. It has also been shown that MD simulations of ligand-functionalized nanoparticles can be used as useful tools for studying interactions of metal nanoparticles with biomolecular species such as nucleic acids,[26] DNA,[27, 28] proteins,[29, 30] and lipid membranes,[31-34] opening up the opportunity for their use in nanomedicine.[3] Fundamental questions remain, however, regarding the structure, preferred conformations and folding of organic polymers or peptides attached covalently to an inorganic core.

Developing of MD models and force field (FF) parameters for gold nanoparticles functionalized by pHLIP is a rather difficult task due to limited sets of high-resolution experimental data available for the peptide structure and folding. In this study, we focus our attention on small nanoparticles built on a gold core with a diameter of 1.4 nm and functionalized by a monomaleimide moiety (Figure 1). This system mimics commercially available a monomaleimido NANOGOLD® labelling agent, which was recently used in a series of anticancer treatment experiments[12] and other biophysical studies.[35-38] Our goal is to benchmark the performance of some standard biomolecular FFs, because this approach also opens the possibility of exploring the interactions between pHLIP-functionalized AuNPs and biologically relevant species such as proteins, DNA, and lipid bilayers without additional FF developing and mixing various FF parameters. Therefore, this study aims at some critical analysis of popular biomolecular force fields: (*i*) five all-atom FFs, including AMBER03, CHARMM22*, CHARMM27, CHARMM36 and OPLS-AA, and (*ii*) one united-atom GROMOS G53A6 FF. For the sake of comparison, OPLS-AA FF simulations were tested in a combination with both explicit TIP3P and implicit General Born water models. Large-scale parallel molecular dynamics simulations of the same system with different FFs were then carried out, including multiple independent start conformations and thermal annealing, so that the total time of MD sampling reaches 1.5 μs. To investigate the performance of individual FFs for peptide–gold interactions, the various structural parameters were calculated for AuNP-pHLIP using each FF and compared to the available experimental data. We demonstrate that unfolded conformations of pHLIP peptide can exist when the peptide is bound to the AuNP surface. Subsequently, through a comparative analysis we show that the most of current popular FF models are able to reproduce the structure of AuNP-pHLIP in aqueous salt solution at neutral pH. We anticipate, therefore, that these findings will be important not only for defining the selectivity of pH-sensitive peptides and the targeted delivery of AuNP-conjugates toward lipid membranes, but also for understanding the role of peptide/gold interactions in modulating of peptide functions or gold binding.

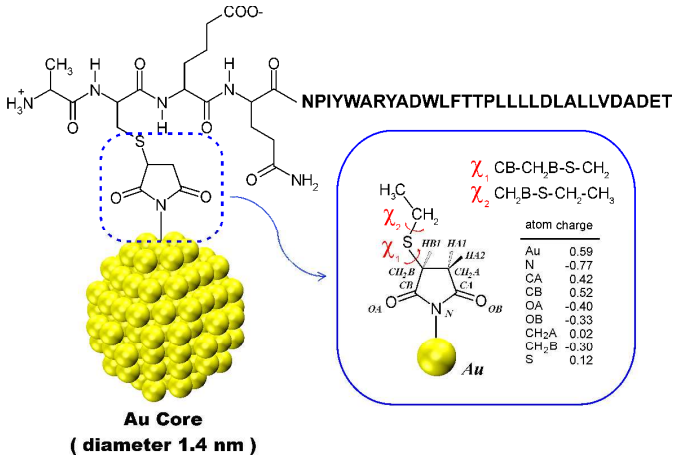

Fig. 1 Molecular Structure of AuNP-pHLIP. A schematic view of covalent coupling of pHLIP peptide to a gold core through a maleimide moiety. The N-terminal part (ACEQ) of pHLIP is coupled to the maleimide fragment through a cysteine residue. The rest of the peptide is shown by the amino acid sequence. The inset shows the molecular structure, labelling scheme, partial charges, and dihedral angles χ1 and χ2 in a gold-maleimido anchoring site.

2. Methods

2.1 Design of Anchoring Site

To develop a new set of bonded force field parameters for a maleimide anchoring site, the geometry of a gold-maleimide-S-CH_2-CH_3 moiety (Figure 1) was optimized by *ab initio* calculations at the UMP2/cc-pVDZ theory level by using the GAMESS software.[39] The LANL2DZ potential[40] was used for the core electrons and the basis set of gold. The bond length and angle parameters for the optimized geometry of the anchoring moiety were adopted for the corresponding force field. The partial electric point charges were estimated on the optimized structure by the electrostatic potential (ESP) calculation utilizing the method of Besler-Merz-Kollman.[41] Using the same level of the MP2 calculations, the scans of the torsion angle χ_1 and χ_2 in an anchoring site linker (Figure 1)

were carried out to adjust parameters for the rotational barrier heights. The final sets of the bonded interactions parameters for the anchoring moiety are given in Table 1.

Table 1 Force field parameters for bonded interactions in gold-maleimide anchoring site.[a]

bond stretch		
bonds	r_{ij} (nm)	K^r_{ij}(kJ/(mol nm^2))
Au-N	0.201	1.87×10^6
N-CA, N-CB	0.139	1.18×10^6
CA-OA, CB-OB	0.122	1.66×10^6
CA-CH_2A, CB-CH_2B	0.153	7.15×10^5
CH_2A-CH_2B	0.153	7.15×10^5
CH_2B-S, S-CH_2	0.182	2.00×10^6
angle bend		
angles	Θ_{ijk} (degree)	K^Θ_{ijk}(kJ/mol)
Au-N-CA, Au-N-CB	123.1	844
CA-N-CB	113.7	465
N-CA-CH_2A, N-CB-CH_2B	107.5	685
N-CA-OA, N-CB-OB	125.5	560
CA-CH_2A-CH_2B	104.5	444
CB-CH_2B-CH_2A	104.5	444
CH_2A-CH_2B-S	116.8	745
CH_2B-S-CH_2	97.8	900
torsion		
dihedrals	φ_{ijkl} (degree)	K^φ_{ijkl} (kJ/mol)	*n*
CB-CH_2B-S-CH_2	175.0	22.0	2
CH_2B-S-CH_2-CH_3	180.0	20.0	2
improper dihedral			
dihedrals	φ_{ijkl} (degree)	K^φ_{ijkl} (kJ/mol)	*n*
CH_2B-S-CA-CH_2A	36.7	200.0	

[a] see Figure1 for atom labeling

2.2 MD Models of AuNP-pHLIP

The systems under consideration consist of a monomaleimido-pHLIP-functionalized gold nanoparticle (AuNP-pHLIP) in aqueous salt solution at neutral pH. Gold nanoparticles were modelled as a quasi-spherical gold core with the face-centered cubic (fcc) crystalline structure composed of the fixed number of 135 gold atoms. The average diameter of such a nanoparticle core equals to 1.4 nm (Figure 1). pHLIP peptide (ACEQNPIY-WARYADWLFTTPLLLLDLALLVDADET) was constructed in random coil conformations and attached to the gold core through the gold-maliemide moiety, as shown in Figure 1. To benchmark a role of the parameterization in determining the protein folding and the equilibrium structure of AuNP-pHLIP in aqueous salt solution at neutral pH, a series of constant pH MD simulations of AuNP-pHLIP were performed with popular, all-atom force fields such as AMBER03[42] and OPLS-AA.[43] Additionally, the performance of the CHARMM family of all-atom FFs (as implemented in the GROMACS package[44]) was also tested. The latter FFs are known as being able to reproduce both the correct native state and the folding for many small peptides and proteins in solution: CHARMM22*[45] with modified backbone torsion potentials; CHARMM27[46] and CHARMM36,[47] the first FF with the CMAP protein backbone correction and the second FF is its extension for lipids and membrane proteins. Furthermore, the structure of AuNP-pHLIP were modelled by using, united-atom parameterizations based on biomolecular GROMOS G53A6 FF,[48] in which some peptide fragments (CH_3, CH_2 and CH) were treated as a single interacting site.

We used water models suggested by the developers of each particular FF. The CHARMM and G53A6 simulations were carried out using TIP3P[49] and SPC[50] water models, respectively. MD simulations of AuNP-pHLIP based on AMBER03 were carried out in a combination with the four-site water model TIP4P/2005,[51] which is characterized by four interaction points by adding one dummy atom near of the oxygen along the bisector of the HOH angle of the three-site models. To neutralize the solution, we use sodium chloride (NaCl) as electrolyte. In all our explicit water simulations, the salt concentration was adjusted to be 100 mM. Table 2 lists the total number of water molecules, buffering ions, as well as MD box sizes for the studied AuNP-pHLIP systems. Additionally, control MD simulations were carried for AuNP-pHLIP with OPLS-AA in implicit water solvent, in which the electrostatic effects of solvent molecules were mimicked by using the Hawkins-Cramer-Truhlar (HTC) Generalized Born (GB) model.[52] The Born radii were calculated the every simulation time step with the following parameters: a cut-off for the calculation of the Born radii was 1.2 nm, the dielectric constant for the implicit water was 78, and the concentration of implicit salt was 100 mM, respectively.

Table 2. Simulation details of various AgNP-pHLIP systems[a]

Force Field	Na^+	Cl^-	number of water molecules	water model	size of simulation box (Å)
AMBER03-AA[42]	30	25	13427	TIP4P/2005[51]	75.0×75.0×75.0
OPLS-AA [43]	30	25	13430	TIP3P [49]	75.3×75.3×75.3
OPLS-AA [43]	-	-	-	GB [52]	75.3×75.3×75.3
CHARMM22*-AA [45]	30	25	13430	TIP3P [49]	75.3×75.3×75.3
CHARMM27-AA [46]	30	25	13430	TIP3P [49]	75.3×75.3×75.3
CHARMM36-AA [47]	30	25	13430	TIP3P [49]	75.3×75.3×75.3
GROMOS G53A6-UA[48]	26	21	11037	SPC [50]	70.8×70.8×70.8

[a] in all simulated systems, a gold core was composed of the fixed number of 135 Au atoms.

For each of the studied FFs, nonbonded interactions parameters for the maleimide anchoring moiety were adopted from appropriate atom types (Examples of topology files for gold-maleimido-pHLIP are available in Supplemental Materials). The repulsion and dispersion terms $V(r_{ij})$ describing nonbonded interactions were computed using the Lennard-Jones 12-6 potential energy function (Equation 1).

$$V_{LJ}(r_{ij}) = 4\varepsilon_{ij}\left(\left(\frac{\sigma_{ij}}{r_{ij}}\right)^{12} - \left(\frac{\sigma_{ij}}{r_{ij}}\right)^{6}\right) \quad (1)$$

Suitable nonbonded interactions potentials for Au were adopted from the recent work of Heinz et al.,[53] in which Au-Au 12-6 LJ interaction potentials (Equation 1, σ=0.2951 nm and ε=21.9006 kJ/mol) were fitted to reproduce densities, surface tensions, and interface properties of crystalline, face-centered cubic gold and

other metals. No restrains were applied between gold atoms, so that the gold core crystalline structure was maintained by their LJ interaction potentials. The Lorentz-Berthelot rules were used[54] to construct the parameter matrix for the non-bonded interactions between gold and other atoms. This combination of FF parameters has commonly been utilized in the AuNP simulation literature and is suitable for this study.[20-22, 25, 34]

2.3 MD Simulation Setup

The systems were solvated by explicit water molecules using the water models as specified for the particular system in Table 2. The size of the water box was chosen to ensure that the systems have at least 20 Å solvation shell from the outermost gold atoms in all directions. All the MD simulations were carried out at a constant number of particles, constant pressure of P = 1 atm, and constant temperature T = 303 K (NPT ensemble). Solvent (water, buffering ions), the protein and gold atoms were each coupled separately to a heat bath at the reference temperature of 303 K, which was kept constant using the velocity rescaling weak coupling scheme[55] with a coupling constant τ = 0.1 ps. The initial atomic velocities were generated with a Maxwellian distribution at the given absolute temperature. Periodic boundary conditions were applied to all three directions of the simulated box. Electrostatic interactions were simulated with the particle mesh Ewald (PME) approach[56] using the long-range cutoff of 0.8 nm. The cutoff distance of Lennard-Jones interactions was also equal to 0.8 nm. The MD simulation time step was 2 fs with the neighbour list updates every 10 fs. All bond lengths in the protein were kept constant using the LINCS routine.[57, 58] The MD simulations were carried out using the GROMACS set of programs, version 4.5.5.[54] Molecular graphics and visualization were performed using VMD 1.8.6.[59]

3. Results and discussion

3.1 pHLIP Structure

pHLIP is a water-soluble peptide derived from the transmembrane helix C of the integral membrane protein Bacteriorhodopsin[6] and composed of 35 amino acids (Figure 1). Folding and functioning of pHLIP depend on pH, therefore, similarly to other proteins, pH affects its structure, dynamics, and function, because the protonation state of the ionizable groups of a protein depends on pH. In most current force fields, however, the protonation state of a peptide (rather than its pH) is kept fixed and cannot adapt to changes of the local protein folding. In a neutral pH (pH 7.0) environment, the side chains of Asp, Glu and *C*-terminus are deprotonated (4 Asp^-, 2 Glu^- and COO^-), and the side chain of Arg and the *N*-terminus are protonated (Arg^+ and NH_3^+). Therefore, pHLIP carries five net negative charges at neutral pH. The presence of protonatable residues, carrying negative charges, is required for guaranteeing solubility of pHLIP in aqueous solutions. Here we performed the constant pH MD simulations, so that a structure of pHLIP with the abovementioned fixed protonation states was used, chosen according to the most probable protonation arrangement at neutral pH.

At neutral and high pH, pHLIP and its mutants are largely unstructured in solution, as demonstrated by numerous circular dichroism (CD) experiments.[7, 8, 60, 61] Therefore, in all the AuNP-pHLIP systems, initial configurations of pHLIP were constructed in random coil extended conformations.

3.2 AuNP-pHLIP Structure

As a first test of system properties, the same system of a single AuNP core functionalized by monomaleimido-pHLIP were simulated in aqueous salt solution at neutral pH using combinations of various protein force fields and water models (Table 2).

3.2.1 AMBER03. Figure 2 shows time-evolution of AuNP-pHLIP estimated by MD simulations using the AMBER03 FF model[42] combined with TIP4P/2005 water.[51] At t=0 ns, the peptide was initially arranged in an extended configuration and the majority of the peptide residues were at distances lager than the cut-off distance of 8 Å used for the Au-to-peptide interactions, so that the peptide was not interacting with the Au atoms. After 20-30 nanoseconds of thermally-driven flipping and diffusion, the peptide refolds and randomly enters the interaction region of the Au surface. We observed that once the peptide approaches close to the inorganic core, the peptide binding and anchoring onto the Au surface occur. After initial peptide/gold interaction events, the binding process continues with the binding of other residues occurring during 40-50 ns of MD sampling. Figure 2*a* shows MD snapshots of time evolution of the peptide folding and interactions with the gold core.

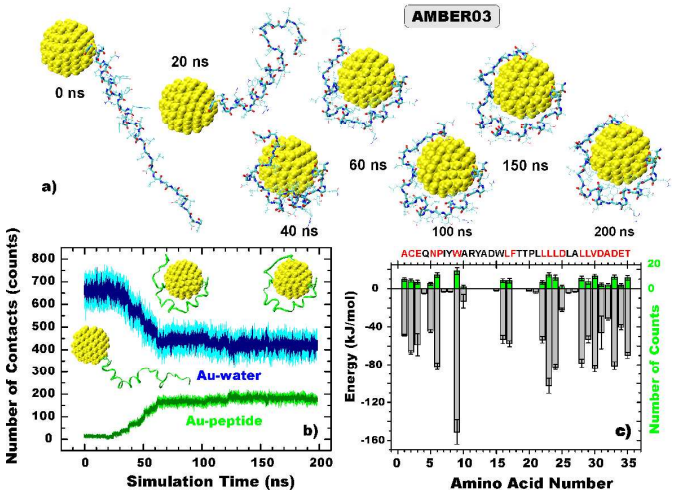

Fig. 2 MD simulation of AuNP-pHLIP with AMBER03: **(a)** MD snapshots were taken at different simulations times showing time evolution of pHLIP adsorption onto a gold core. The gold core (*yellow*) is drawn in van-der-Waals representations and shown in the same orientation for clarity. pHLIP backbone is drawn *green* in a licorice mode. Water molecules and buffering ions are not shown. (**b**) The time variations of the number of the neighbouring contacts Au-to-water (*cian*) and Au-to-peptide (*green*). Solid *blue* and *olive* curves represent smooth-averaged data for each 50 trajectory points. The insets show MD snapshots of representative configurations of AuNP-pHLIP. (**c**) Bar plots of

adsorption energies and the number of contacts between the gold core and individual amino acids of pHLIP. Top label shows pHLIP's sequence in which strongly bound residues are colored *red*.

We found that there is no adsorption selectivity for any part of the peptide onto gold at this stage. During the first stage, a series of the changes and rearrangements in the peptide's configuration happen until pHLIP finds an appropriate configuration and position to anchor or bind. The flexibility of the peptide's backbone is crucial at this stage. With time, some of the pHLIP residues found their way to the gold surface and displace some interfacial water molecules, becoming adsorbed onto the surface.

Various structural parameters were analyzed during the course of pHLIP adsorption onto a gold nanoparticle core. More details of the peptide-gold interactions are given in Figure 2*b* showing the time evolution of the number of the neighbouring contacts Au-to-water and Au-to-pHLIP, respectively. The atoms of either water or the peptide were defined to be within a neighbouring contact with the gold surface when their distance to the outermost Au atoms was less than 3.5 Å. The choice of the precise value of this threshold is somewhat arbitrary, so that the cut-off value of 3.5 Å was chosen on the basis of the first peak positions in radial distribution functions (RDF), estimated between the Au atoms and either the oxygen or the nitrogen atoms of pHLIP, considered as the major anchoring sites.

Figure 2*b* shows that, upon pHLIP adsorption onto gold, the number of the neighbouring contacts between the gold atoms and water molecules is gradually decreased from 670±40 to 435±36 during the first 60 ns. This decrease is accompanied by the rapid increase in the number of the neighbouring contacts between Au and pHLIP occurring in the same time scale. The number of the contacts between Au and pHLIP fluctuated significantly due to the peptide flexibility on the surface (see Figure 2*b*). After 80 ns, both curves demonstrate some plateau and random fluctuations around some average values, indicating that the system AuNP-pHLIP reaches the equilibrium state. This equilibration effect is clearly seen when the curves are smoothed as shown by solid lines in Figure 2*b*. The simulations were, therefore, run until the number of the contacts Au-to-pHLIP, and, hence, the number of the adsorbed residues remained constant for at least 50 ns. At equilibrium, the average number of the contacts Au-to-pHLIP was found to be 183±9. The trends in the number of the contacts Au-to-water and Au-to-pHLIP correlated with the observed events of peptide adsorption onto the gold core (Figure 2*a*).

The effect of pHLIP adsorption onto a gold core is further explored in Figure 2*c*, which shows the correlation between the number of the neighbouring contacts to gold and the adsorption energy for each individual peptide residue with the gold surface. The adsorption energies were calculated as sum of pair-wise nonbonded Lennard-Jones energies acting between all residue atoms and gold atoms found within the simulation cut-off distance of 8 Å.

The bar plots shows that this correlation is consistent with a physical picture in which the peptide binds onto gold through some anchoring residues confined by steric interactions with adjacent side chains. Figure 2*c* shows that the strongest bound residue was tryptophan W9, which rigidly anchored the whole N-terminus part of the peptide onto the gold surface.

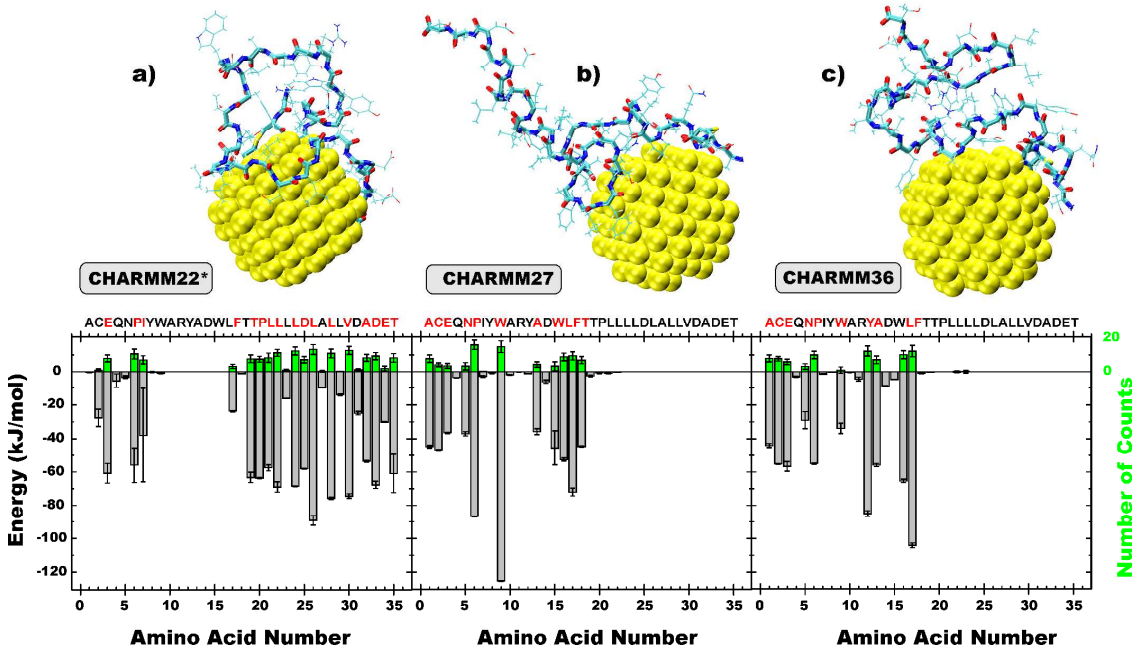

Fig. 3 Adsorption Energy estimated by using various CHARMM FFs: Final MD snapshots of AuNP-pHLIP estimated by three variants of CHARMM FFs: (**a**) CHARMM22*-AA, (**b**) CHARMM27-AA, (**c**) CHARMM36-AA. (*Bottom Panels*) Bar plots of adsorption energies and the number of the direct contacts between the gold core and individual amino acids in AuNP-pHLIP estimated by MD simulations using the corresponding CHARMM FFs: Top labels show pHLIP's sequence in which the strongly bound residues are colored *red*.

3.2.2 CHARMM FFs. The same general trends in pHLIP adsorption onto gold, previously reported in Figure 2 for the AMBER03 FF model, were also observed upon MD simulations based on the CHARMM family of all-atom FFs. First, a rapid initial anchoring of the peptide onto the gold surface occurs, which is followed by crawling and gradual wrapping of the peptide around an inorganic core (Supplemental Figures S1-S2). These events were then followed by peptide backbone rearrangement and tight binging to the gold surface. The major distinctions in the adsorption behaviour predicted by various CHARMM FFs were mainly observed in the initial anchoring events, the bound peptide parts, and chain positions of the strong binding residues. According to all CHARMM MD models, pHLIP was partially bound onto the gold surface thought some short hydrophobic peptide stretches, while large peptide fragments remain in aqueous salt solution. For CHARMM22*, pHLIP adsorption behaviour is shown in more detail in Supplemental Figure S1.

Figure 3 shows the correlation between the number of the contacts to gold and the adsorption energy with the gold core for each amino acid residue. The three CHARMM FF models lead to some different predictions concerning the peptide's adsorption onto the gold nanoparticle core: According to the CHARMM22* prediction, pHLIP binds and adsorbs onto the gold by the C-terminal part composed of residues 18-35 (Supplemental Figure S1 and Figure 3*a*). At the same time, both CHARMM27 and CHARMM36 simulations revealed that the peptide is adsorbed onto gold due mainly to the N-terminal fragment composed of residues 5-17. Therefore, the two latter FF models predict that the C-terminal fragment of pHLIP remains unbound to gold and soluble in aqueous salt solution. All studied CHARMM FF models predicted that the surface bound and unbound parts of the peptide appear to be exposed toward aqueous salt solution and their structure is completely unfolded and disordered.

The simulations based on the CHARMM22* model show that the most residues (18-35) in the C-terminal part of the peptide are tightly bound to gold, as seen in Figure 3*a* from the corresponding adsorption energies. The same trend was also observed in the number of the contacts between each amino acid and gold (Supplemental Figure S1 and Figure 3*a*). On top panels of Figure 3, pHLIP's sequence is given in which the strongly bound residues coloured in *red*. The residue was considered as strongly bound if its negative adsorption energy is > 20 kJ/mol. In the case of the CHARMM27 FF model, a closer examination of the adsorption energies reveals the presence of the strongest binding sites such as P6 and W9. On the other hand, another set of the strong gold-bound residues, such as the residues Y12 and F17, were identified according to the CHARMM36 FF model. The overall strength of intermolecular interactions between pHLIP and gold can also be derived from the average number of the Au-to-pHLIP contacts which are found to be 149±9, 82±7, and 77±7, as estimated by three different FFs: CHARMM22*, CHARMM27, and CHARMM36 FFs, respectively. We also did the transferability test of MD simulations of AuNP-pHLIP by using the different versions of the CHARMM FFs as shown in Supplemental Figure S3. More details of the protein-gold interactions are also summarized in Supplemental Tables S1-S2.

3.2.3 OPLS-AA. Figure 4 shows MD results for the same system of a single AuNP core functionalized by mono–maleimido-pHLIP simulated in aqueous salt solution at neutral pH using a combination of the OPLS-AA FF and TIP3P water model. These results reproduce the same general trends in pHLIP adsorption onto gold, which were observed in the cases of the other studied FF models. The OPLS-AA FF model predicts a rather slow initial anchoring of the peptide onto the gold surface occurring in a time range up to 150 ns (Figure 4*b*). After the initial anchoring, the peptide becomes partially wrapped around an inorganic core as seen in Figures 4*a*-*b*. The OPLS-AA simulations predict that the peptide adsorbs onto gold mainly by its two segments composed of residues 6-12 and 20-23, respectively (Figure 4*c*). In this respect, the peptide adsorption behaviour is similar to those of predicted by the CHARMM27 and CHARMM36 FF models (Supplemental Figure S2 and Figures 3). The average number of the contacts Au-to-pHLIP was found to be 125±8.

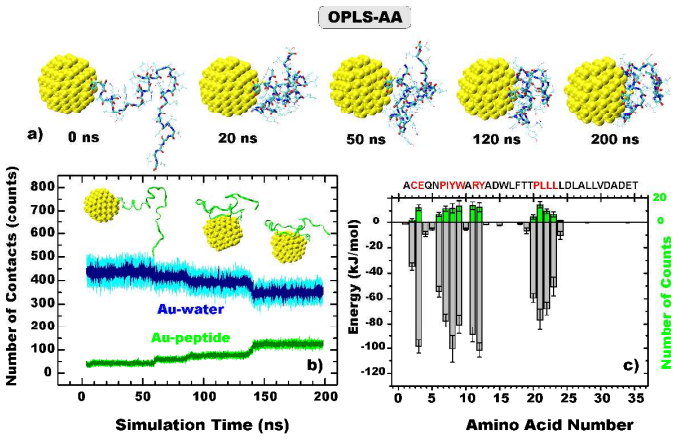

Fig. 4 MD simulation of AuNP-pHLIP with OPLS-AA: **(a)** MD snapshots were taken at different simulations times showing different stages of pHLIP adsorption onto a gold core. (**b**) The time variations of the number of the neighbouring contacts Au-to-water (*cian*) and Au-to-peptide (*green*). The insets show MD snapshots of representative configurations of AuNP-pHLIP. (**c**) Bar plots of adsorption energies and the number of direct contacts between the gold core and individual amino acids of pHLIP. (See Legend for Figure 2 for more detail).

Currently, one of alternative ways to simulate protein folding dynamics and protein structure predictions with atomic resolution using long-scale MD simulations is the use of implicit solvent models, which can dramatically accelerate folding due to lower viscosity that facilitates chain diffusion.[62-65]

Figure 5 compares the structure of AuNP-pHLIP predicted by MD samplings carried out using OPLS-AA in the explicit TIP3P water and implicit water represented by a GB model.[52] The later calculates solvation effects using a continuum representation. Intermediate MD snapshots of AuNP-pHLIP

simulated in the implicit GB water model using the OPLS-AA FF are shown in Supplemental Figure S4. Two interesting observations emerge from the comparison of these structures: (*i*) the peptide chain is exposed toward bulk water upon MD simulations carried out in explicit water, while the peptide chain is well packed and collapsed onto the gold core according to the sampling in the GB model. (*ii*) in the both cases, the peptide adsorbs onto gold through some hydrophobic stretches only, so that its other unbound parts remain unfolded and exposed toward aqueous salt solution.The histograms of the radius of gyration estimated in explicit and implicit waters have further demonstrated differences in gold-bound pHLIP folding. The compact globular structure with the average radius of 9.7 Å was observed in GB water, as compared to the broad histogram peak centred at 11.6 Å, which is characteristic for unstructured and unfolded conformations of the peptide in explicit water.

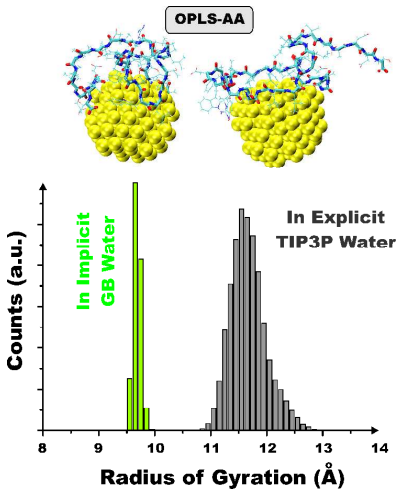

Fig. 5 Comparison of OPLS-AA Simulations in Explicit *versus* Implicit Water: Comparison of the structure of AuNP-pHLIP estimated after MD simulations using the OPLS-AA FF model combined with either explicit TIP3P water (*right*) or implicit GB water (*left*) models, respectively. The snapshots were taken at the end of 200-ns long MD sampling. In the snapshot taken from the explicit water simulations, water molecules and buffering ions are not shown for clarity. Histograms of the radius of gyration of the peptide in AuNP-pHLIP show different compactness of the peptide, as estimated due to applying the two different solvation models.

The previous results show the critical role that the particular force field plays in determining the adsorption behaviour of the peptide due to the different balance between hydrophobic and hydrophilic character of some amino acids. Another factor that might influence the pHLIP adsorption is the initial local peptide folding. To test whether any differences in AuNP-pHLIP properties emerge from changing the peptide folding, we generated a series of random initial peptide configurations. In each of the three different randomly generated starting configurations of the peptide, none of the peptides had fully adsorbed onto the gold surface after 100 ns of unrestrained dynamics using the OPLS-AA/GB formalism.

3.2.4 GROMOS G53A6. Figure 6 shows the analysis of the MD trajectories which provides the amino-acid-specific trends to guide the behaviour of AuNP-pHLIP as examined with the G53A6 united-atom FF model. In an initial configuration, the peptide was also attached to gold in an extended conformation. Our simulations revealed that pHLIP adsorbed rapidly and become wrapped around a spherical inorganic core during the first 50 ns (Figure 6*b*). Upon adsorption, the peptide displaces some interfacial water molecules from the gold surface, so that the number of the contacts Au-to-water was decreased from an initial value of 500±45 up to 230±60, respectively. After adsorption, the peptide appears mostly "glued" to the gold nanoparticle core and restrains significantly its conformational flexibility on the surfaces (Figure 6*b*). At the equilibrium configuration detected at the end of the MD sampling, the average number of the contacts Au-to-pHLIP was found to be 109±8. Figure 6c shows that the amount of the direct contacts with the metal surface correlates with the adsorption energy. In the peptide, we can identify binding residues, (the corresponding residue code is highlighted in *red* in Figure 6*c*), while the remaining residues, coloured in grey, are less binding or nonbinding. According to the G53A6 model, the majority of the peptide residues are found to be in direct contact with the surface, mostly driven by the W9 residue, as well as Y8 and Y12, and the whole C-terminal fragment.

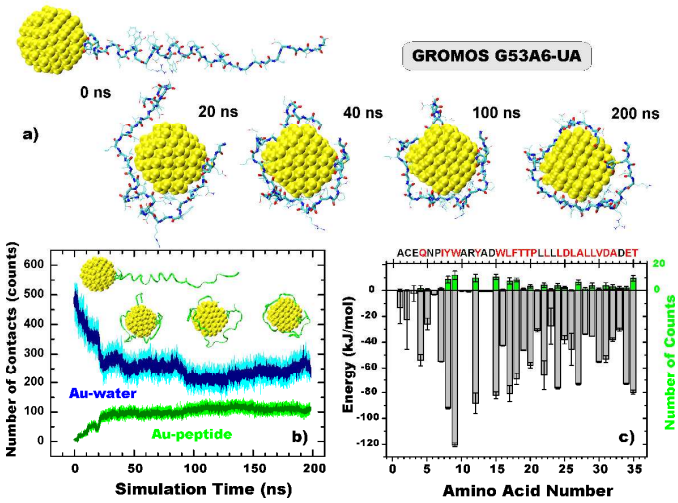

Fig. 6 MD simulation of AuNP-pHLIP with G53A6-UA: **(a)** MD snapshots were taken at different simulations times to monitor pHLIP adsorption onto a gold core. (**b**) The time variations of the number of the neighbouring contacts Au-to-water (*cian*) and Au-to-peptide (*green*). The insets show MD snapshots of representative configurations of AuNP-pHLIP. (**c**) Bar plots of adsorption energies and the number of contacts between the gold core and individual amino acids of pHLIP. (See Legend for Figure 2 for more detail).

It appears that G53A6 overestimates the hydrophobic behaviour of pHLIP. The peptide leaves polar bulk water and favours to minimize water contacts through adsorption onto gold. Recently, Nawrocki and Cieplak have discussed in more detail a role of hydrophilic *versus* hydrophobic FF contributions in favouring adsorption of native amino acids onto a flat gold surface.[66]

3.3 pHLIP Anchoring Sites

The basis for the non-bonded interaction between gold and peptides is related to the high-affinity of some chemical groups of certain amino acids for preferential binding to a gold surface. Therefore, the affinity of a whole peptide to bind to gold depends on the presence and relative propensity of naturally occurring amino acids.[67] There is no well-established experimental scale to measure gold affinity of individual amino acids. However, positively-charged and aromatically rich residues such as Arg, Trp, Tyr, and His, are most frequently mentioned among natural amino acids known as strong Au-binding sites.[68-70] On other hand, real-time surface plasmon resonance (SPR) measurements showed that small aliphatic and negatively charged residues usually reveal a weak potency of Au binding.[69] Numerous computational studies have shown that overall peptide adsorption preferences to gold could not be inferred directly from amino acid adsorption preferences alone, because there is strong interplay between peptide sequence and favourable 3D peptide conformations.[71-74] Additional factors, such as peptide flexibility, crystal facets, and a shape of a nanostructured gold surface, may affect peptide binding to gold.[71, 75-79] Moreover, it has been shown that there is the barrier to peptide adsorption to gold surface caused by displacement of interfacial water molecules.[80]

Figure 7 summarizes the structure of AuNP-pHLIP and the peptide folding as estimated by the various studied FF models. In each structure, two sets of bound and unbound pHLIP residues were shown in *red* and *silver* CPK representations, respectively. In cases of strong binding, individual side groups or backbone residues of pHLIP were found in direct contact with the metal surface, without intermediate water molecules between the peptide and the metal surface. The visualization shown in Figure 7 supports that the peptide adsorbs onto gold so that its backbone may be suitable to form water-assessable loops to connect more specialized strongly-binding fragments. The correlation between adsorbed conformations of the peptide and corresponding adsorption energies further indicates some cooperativity between adjacent amino acids. It should also be pointed out that we found little evidence of direct interactions between buffering ions and Au atoms, preventing or disrupting peptide adsorption onto a nanoparticle core, in agreement with the relatively weak adsorption of chloride ions onto gold observed experimentally and predicted from DFT calculations.[81]

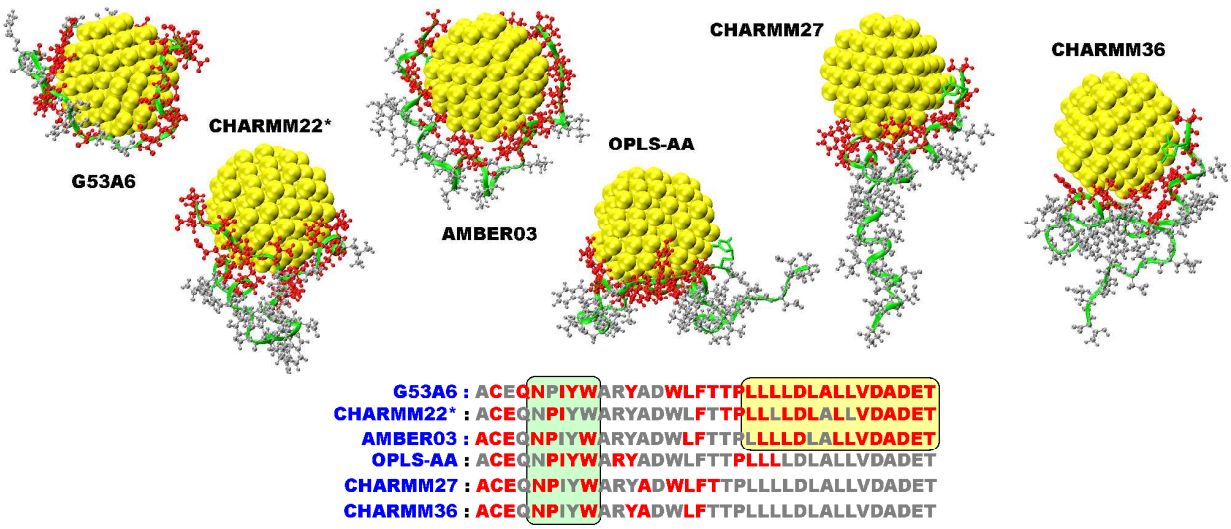

Fig. 7 Anchoring Site Analysis for pHLIP onto Gold Nanoparticle: (*Top*) Typical pHLIP conformations adsorbed onto AuNP are shown as estimated by the various studied FF models. In each case, the peptide backbone is drawn *green* and the anchor residues are shown in CPK representation highlighted *red*. The unbound peptide residues are also shown and highlighted *silver*. Waters and buffering ions are not shown for clarity. (*Bottom*) Summary of pHLIP anchoring sites is given by the peptide sequence in which the surface contact residues are highlighted *red*.

The comparison of the various studied FF models exhibits some interesting trends. Most notably, the binding potential of pHLIP to gold is highest according to G53A6, CHARMM22*, and AMBER03, respectively. Twenty to twenty eight residues, including the whole C-terminal group, bind to gold (highlighted in *yellow* area in Figure 7*bottom*), and only some residues near the centre of the chain favour a water interlayer and detach from the surface. As a result, twelve or fifteen consecutive residues toward the C-terminal end bind to gold.

In the contrast to all these observations, according to OPLS-AA, CHARMM27 and CHARMM36, pHLIP was predicted as being essentially inert against the gold surface and shows adsorption through certain point-anchoring residues on the AuNP surface. The peptide interacts slightly with gold, which results in minor adsorption through five or six residues only, and other partial contacts, including the N-terminal attachment moiety. The water-soluble peptide fragments resist flattening of the rest of the peptide backbone onto the gold surface, so that more than half the peptide chain residues remains water exposed (Figure 7).

3.4 Trp-to-Au Distances

Changes of tryptophan fluorescence are commonly used to monitor pHLIP folding in solution, its aggregation, and binding to a membrane lipid bilayer at neutral pH, as well as its bilayer insertion at lower pH.[7, 60, 61, 82] It has, however, been found that, when pHLIP was covalently coupled to NANOGOLD, its tryptophan fluorescence was significantly quenched, pointing out to the close proximity of the tryptophan residues to the inorganic core.[12] Recently, it has also been shown that both steady state fluorescence and lifetime measurements of protein-protected gold nanoclusters revealed a significant Forster Resonance Energy Transfer (FRET) from Trp residues to a gold core, so that the apparent distances between Trp and a gold nanocluster centre was estimated to be in a range 23.8 Å - 24.8 Å.[83] While quenching mechanisms of native Trp fluorescence in biopolymers bound onto AuNPs still remain under active debates, several lines of evidences indicate that when Trp residues approach gold nanocrystals its emission become strongly decreased.[84]

We now, therefore, turn our attention to the analysis of the distances Trp-to-gold, which are the most valuable pieces of information provided by the simulations in terms of experimental validations.[12] Figure 8 shows the time traces of the shortest distances between pHLIP's tryptophan residues and the outermost gold atoms in AuNP-pHLIP calculated by three different FF models. To determine the shortest distance we consider the closest contacts appeared between all Trp atoms and the outermost gold atoms. pHLIP contains two Trp residues, so that the distances to gold are separately plotted for two residues W9 and W15, respectively. As seen from Figure 8, the adsorption behaviour of W9 and W15 onto gold correlates well with overall adsorption behaviour of the whole peptide simulated with the corresponding FF models (Figures 2, 3-4, 6).

MD simulations using the CHARMM22* model revealed that, after initial anchoring of pHLIP to the gold core, both W9 and W15 remain loosely bound to the gold surface as evident from high amplitude fluctuations of the distances between Trp

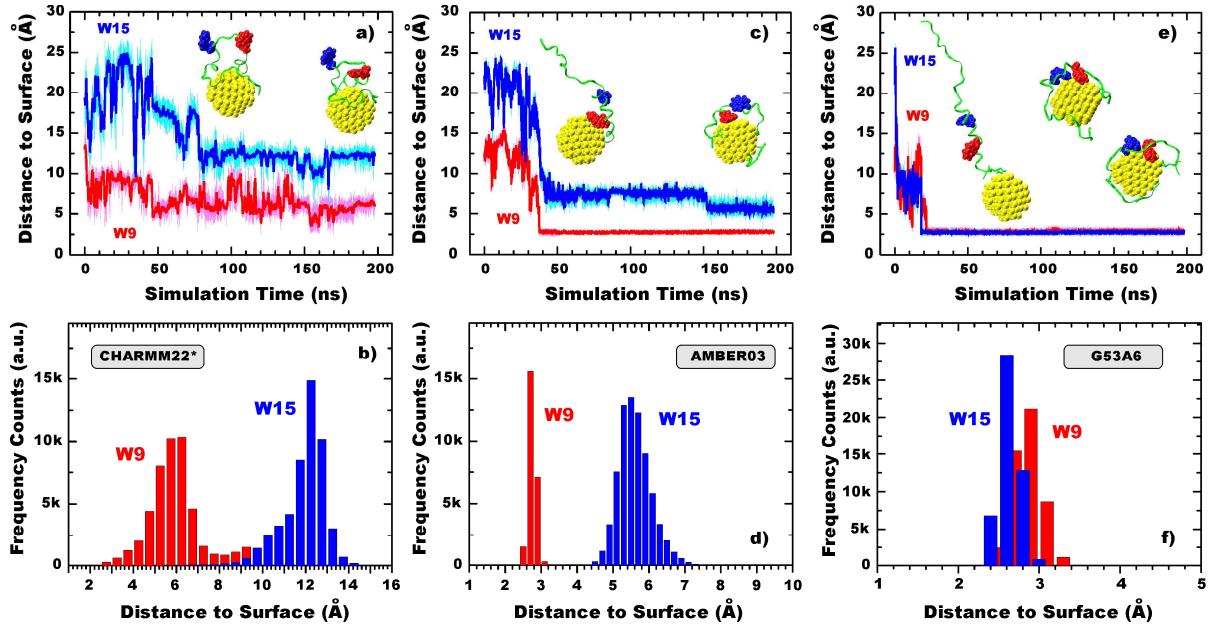

Fig. 8 Trp-to-Gold Distances: The time-traces of the shortest distance between pHLIP tryptophan residues W9 (*red*), W15 (*blue*) and the gold surface calculatedfor AuNP-pHLIP using the various studied FFs. The insets show MD snapshots of AuNP-pHLIP in which the peptide is drawn as *green* ribbon and the Trp residues are shown in the colour-coded vdW representation. The histograms of the distance distributions W9-to-gold (*red*) and W15-to-gold (*blue*) estimated for the last 100 ns of the MD sampling: (**a**-**b**) MD simulations using CHARMM22*; (**c**-**d**) AMBER03; (**e**-**f**) G53A6.

and gold, as well as peak positions and widths of the corresponding distance distribution histograms shown in Figure 8*a*-*b*. In contrast, we observed that only residue W9 became tightly bound to gold and remains rigidly fixed on the gold surface after 40 ns simulations using AMBER03 FF. It is interesting to note that, already after 30 ns, both residues W9 and W15 become tightly bound to the gold surface, as predicted by MD samplings with G53A6 FFs. The analysis of the tightly-bound Trp configurations revealed that, in order to minimize its water accessible surface area, the aromatic ring of Trp residues have full contact with the gold surface. The Trp ring adsorbs onto the gold surface in an almost flat sidechain orientation. Such Trp adsorption behaviour has previously been reported from combined DFT and MD simulation studies for an isolated Trp residue on a gold(111) surface.[85]

Table 3 summarizes the distances Trp-to-gold estimated by all studied FFs, which were trajectory-averaged for the last 100 ns of the MD samplings. Precise experimental verifications of these Trp-to-gold distances are not available. However, all the studied FF models of AuNP-pHLIP predicted that the most Trp-to-gold contacts are found to be within the distance range

in which the strong fluorescence quenching of Trp emission might occur.

Table 3. Average distances Trp-to-Gold (in Å) estimated by MD simulations using the studied force fields.

Force Field/Water Model	W9-to-Au	W15-to-Au
AMBER03/TIP4P2005	2.7±0.2	5.5±0.3
OPLS-AA/TIP3P	2.7±0.1	5.7±0.6
OPLS-AA/GB	2.5±0.1	2.3±0.1
CHARMM22*/TIP3P	6.1±0.3	12.3±0.3
CHARMM27/TIP3P	2.9±0.2	5.9±0.4
CHARMM36/TIP3P	5.5±0.2	5.8±0.3
G53A6/SPC	2.9±0.2	2.7±0.2

3.5 Radial Distribution Functions

In the case of spherically symmetric systems such as ligand-decorated metal nanoparticles, fine structure details of assembling and packing of ligands or polymers can be extracted by analyzing the three-dimensional radial distribution functions (RDF) calculated from either the nanoparticle surface or its centre. Therefore, we calculated RDF mass profiles of the peptide with respect to the gold surface for all the studied FF models as shown in Supplemental Figure S4. The RDF profiles were evaluated for the last 20 ns of MD sampling of each system. The broad RDF peaks indicate the highly heterogeneous configurations of the backbone and side chains of the adsorbed peptide, which agree well with the MD simulation snapshots shown in Figures 2-8. The peak position of the peptide is centered at distances 16-17 Å from the gold core surface. Therefore, despite of some variations in the observed residue-specific adsorption behaviour of pHLIP onto AuNP, the six different force fields investigated here were all able to reproduce the physical picture: the peptide adsorbs onto gold in unfolded and unstructured conformations, and in the bound conformations it keeps the very similar bulk shape, as predicted by RDF mass density profiles shown in Figure S5. Additionally, no α-helical structure was found and the peptide adsorbs rather as a compact random coil. These findings agree well with CD experimental observations that in pHLIP-NANOGOLD conjugates the peptide exist in unfolded conformations.[51]

3.7 Comparison of FF Models

Molecular dynamics simulations have complemented nicely experimental measurements and provided new insight into many fields of biomolecular simulations, as well as modelling of intermolecular interactions occurring at organic/inorganic interfaces.[28, 86, 87] However, numerous computational studies have also demonstrated that the quality of theoretical data might dramatically depends on the quality of force field parameters, making experimental verification of the simulations extremely important.[66, 88-93]To date, numerous FFs have been developed for short peptide and proteins, mostly focusing on reproducing their structure and native folding in solution.[52, 53, 86] This is the reason why advanced atomistic FFs compatible with protein FFs would be a promising tool to describe the behaviour of the protein within realistic complex nanoconjugates. Using the standard biomolecular force fields leaves also open the possibility of exploring the interactions between pHLIP-functionalized AuNPs and biologically relevant species such as proteins, DNA, and lipid bilayers without additional FF developing and mixing various force field parameters.

The same system AuNP-pHLIP, with otherwise identical MD simulation parameters, shows the behaviour similar in many aspects: the peptide pHLIP was partially adsorbed to the inorganic gold core and remained completely unfolded and disordered. Depending on the used FFs, there were also some minor differences in the peptide chain positions of the bound segments and binding strength of individual amino acids. Unfortunately, we cannot verify this difference against experiment directly. Even without some solid high-resolution structural information about peptide conformations, unfolded structure of pHLIP, covalently coupled to a gold nanocrystal, was reproduced by all the studied FFs. However, some verification is still available for pHLIP folding: the CD results indicate that the gold-bound peptide exists in random coil conformations,[12] consistent with our MD predictions. As expected, a change from all-atom to united-atom G53A6 parameterizations certainly shifted the hydrophobic-hydrophilic balance. Thus, the probable reason for the differences in peptide folding onto the surface is not the protein force field, but rather some imbalance between gold-protein and protein-water force fields. More validations are clearly necessary to investigate these issues.

The overall reliability of the peptide-gold force field warrants discussion. Unfortunately, unlike the case of some short gold-binding peptides,[68-70] we do not have solid experimental structural data for AuNP-pHLIP system available for comparison. In our case, the force field describing an inorganic gold core are based on Lennard-Jones 12-6 potentials[53] and zero partial charges distributed over atomic Au sites, whereas biomolecule force fields typically use protein folding adapted FFs. In such a case, straightforward application of the Lorentz-Berthelot mixing rules for nonbonded interactions may give overestimated adsorption behaviour, because of the lack of harmonization between the LJ potentials operating between organic and inorganic components. However, in our case the gold component of our force field was designed with this harmonization in mind as has been shown for simulations of many similar nanosystems.[20, 23, 25] Therefore, it is still not clear whether some structure variations of the adsorbed peptide conformations observed during MD sampling might be caused by insufficient parameterization or deficiency in the computational models due the use of the simple forms of force fields potentials. Nevertheless, although the experimental data necessary to validate our MD models of AuNP-pHLIP exhaustively are not always available, we believe that our current FF models are able to capture the physics and chemistry of the pHLIP−gold interface.

4. Summary and Future Perspective

Recent advances in gold technology have led to appearance of gold reagents with improved physicochemical properties and better performance for labelling, sensitivity, and functioning, opening up the opportunities for chemical crosslinking of gold particles to many biologically active molecules, such as peptide, proteins, and lipids.[35] For widening the arsenal of gold-peptide therapeutics that act within cells, the structure of gold-nanoconjugates, peptide-gold interactions, peptide folding and adsorption distribution need to be characterized in detail. In this study, we focused our attention on small gold nanoparticles functionalized by a monomaleimide moiety with a core diameter of 1.4 nm. Such a gold nanoparticle mimics commercially available a monomaleimido NANOGOLD® labelling agent, which was recently used in a series of anticancer treatment experiments.[12, 94]

To probe structure and dynamics of gold nanoconjugates, we have developed of a series of MD models for gold nanoparticles functionalized by pHLIP. We have performed the comparative analysis of a series of the popular biomolecular FFs: five all-atom FFs have been evaluated, including AMBER03, CHARMM22*, CHARMM27, CHARMM36 and OPLS-AA. In addition, one united-atom GROMOS 53A6 FF has also been benchmarked for comparison. We found that according to the CHARMM and OPLSAA FF models, pHLIP was found to be partially bound onto the gold surface thought some short hydrophobic peptide stretches, while large peptide fragments remain in aqueous salt solution at neutral pH. In contrast, AMBER03 and G53A6 FFs predicted the formation of compact, tightly bound peptide configurations adsorbed onto the nanoparticle core. Despite of some observed variations in the residue-specific adsorption behavior for pHLIP onto AuNP, to reproduce the physical picture of the peptide adsorption onto gold in unfolded and unstructured conformations our work provides some recommendations and the ready-to-use MD models based on CHARMM36 and OPLS-AA FFs as a tool of choice for computational studies of NANOGOLD decorated by pHLIP peptide.

In our main conclusions we show that several factors such as the amino acid sequence, the molecular architecture of the studied peptide and the morphology of quasi-spherical crystalline gold core are key determinants for the selective binding of pHLIP onto gold. Therefore, the selection of the force field that best agrees with the experimental data appears to be non trivial. Although we are aware that our results can be limited by the accuracy of the force fields, the computational time, and the conformational sampling of the peptides, the MD simulations still proved to be suitable to explain the behaviour of the gold-bound peptide that was previously observed experimentally. Nevertheless, due to the complexity of a system composed by an inorganic surface, a protein and water, a systematic approach used in our work and based on a classical atomistic MD study of the system seems the best compromise between computational accessibility and capability of correctly catching the physical chemistry of the system. In recent years, several groups have probed biomolecule-gold adsorption using advanced computational techniques and a series of problem-specific FFs, such as GolP[95] and GolP-CHARMM,[96, 97] respectively. These approaches, designed to capture the facet selective protein adsorption onto either Au(111) or Au(100) interfaces, as well as taking into account the gold surface charges and polarization, can be considered as promising improvements of current FF models for AuNP-pHLIP nanoconjugates.

Acknowledgements

This work was performed using computational facilities of the joint computational cluster of SSI "Institute for Single Crystals" and Institute for Scintillation Materials of National Academy of Science of Ukraine incorporated into Ukrainian National Grid. The author acknowledges the grant 0113U002426 of Ministry of Education and Science of Ukraine.

References

1. E. C. Dreaden and M. A. El-Sayed, *Acc. Chem. Res.*, 2012, **45**, 1854-1865.
2. Z. Cheng, A. Al Zaki, J. Z. Hui, V. R. Muzykantov and A. Tsourkas, *Science*, 2012, **338**, 903-910.
3. E. C. Dreaden, A. M. Alkilany, X. Huang, C. J. Murphy and M. A. El-Sayed, *Chem. Soc. Rev.*, 2012, **41**, 2740-2779.
4. J. F. Dorsey, L. Sun, D. Y. Joh, A. Witztum, A. A. Zaki, G. D. Kao, M. Alonso-Basanta, S. Avery, A. Tsourkas and S. M. Hahn, *Translational Cancer Research*, 2013, **2**, 280-291.
5. B. Kang, M. A. Mackey and M. A. El-Sayed, *J. Am. Chem. Soc.*, 2010, **132**, 1517-1519.
6. O. A. Andreev, A. D. Dupuy, M. Segala, S. Sandugu, D. A. Serra, C. O. Chichester, D. M. Engelman and Y. K. Reshetnyak, *Proc. Natl. Acad. Sci. U.S.A.*, 2007, **104**, 7893-7898.
7. Y. K. Reshetnyak, M. Segala, O. A. Andreev and D. M. Engelman, *Biophys. J.*, 2007, **93**, 2363-2372.
8. M. Zoonens, Y. K. Reshetnyak and D. M. Engelman, *Biophys. J.*, 2008, **95**, 225-235.
9. L. Han, H. Ma, Y. Guo, Y. Kuang, X. He and C. Jiang, *Adv. Healthcare Materials*, 2013, **2**, 1435-1439.
10. E. A. Sosunov, E. P. Anyukhovsky, A. A. Sosunov, A. Moshnikova, D. Wijesinghe, D. M. Engelman, Y. K. Reshetnyak and O. A. Andreev, *Proc. Natl. Acad. Sci. U.S.A.*, 2013, **110**, 82-86.
11. D. Wijesinghe, M. C. M. Arachchige, A. Lu, Y. K. Reshetnyak and O. A. Andreev, *Scientific Reports*, 2013, **3**, 3560-1/3560-7.
12. L. Yao, J. Daniels, A. Moshnikova, S. Kuznetsov, A. Ahmed, D. M. Engelman, Y. K. Reshetnyak and O. A. Andreev, *Proc. Natl. Acad. Sci. U.S.A.*, 2013, **110**, 465-470.
13. J. C. Deacon, D. M. Engelman and F. N. Barrera, *Archiv. Biochem. Biophys.*, 2015, **565**, 40-48.
14. A. Davies, D. J. Lewis, S. P. Watson, S. G. Thomas and Z. Pikramenou, *Proc. Natl. Acad. Sci. U.S.A.*, 2012, **109**, 1862-1867.
15. O. A. Andreev, D. M. Engelman and Y. K. Reshetnyak, *Frontiers in Physiology*, 2014, **5**, 1-7.
16. D. J. Lewis and Z. Pikramenou, *Coord. Chem. Rev.*, 2014, **273–274**, 213-225.

17. Z. Zhao, H. Meng, N. Wang, M. J. Donovan, T. Fu, M. You, Z. Chen, X. Zhang and W. Tan, *Angew. Chem., Int. Ed.*, 2013, **52**, 7487-7491.
18. P. K. Ghorai and S. C. Glotzer, *J. Phys. Chem. C*, 2010, **114**, 19182-19187.
19. A. Kyrychenko, G. V. Karpushina, S. I. Bogatyrenko, A. P. Kryshtal and A. O. Doroshenko, *Comput. Theor. Chem.*, 2011, **977**, 34-39.
20. E. Heikkilä, A. A. Gurtovenko, H. Martinez-Seara, H. Häkkinen, I. Vattulainen and J. Akola, *J. Phys. Chem. C*, 2012, **116**, 9805-9815.
21. A. Kyrychenko, G. V. Karpushina, D. Svechkarev, D. Kolodezny, S. I. Bogatyrenko, A. P. Kryshtal and A. O. Doroshenko, *J. Phys. Chem. C*, 2012, **116**, 21059-21068.
22. R. C. Van Lehn and A. Alexander-Katz, *J. Phys. Chem. C*, 2013, **117**, 20104-20115.
23. G. Milano, G. Santangelo, F. Ragone, L. Cavallo and A. Di Matteo, *J. Phys. Chem. C*, 2011, **115**, 15154-15163.
24. A. Kyrychenko, O. M. Korsun, I. I. Gubin, S. M. Kovalenko and O. N. Kalugin, *J. Phys. Chem. C*, 2015, **119**, DOI: 10.1021/jp510369a.
25. T. Mandal, C. Dasgupta and P. K. Maiti, *J. Phys. Chem. C*, 2013, **117**, 13627-13636.
26. T. I. N. G. Li, R. Sknepnek, R. J. Macfarlane, C. A. Mirkin and M. Olvera de la Cruz, *Nano Lett.*, 2012, **12**, 2509-2514.
27. O.-S. Lee, T. R. Prytkova and G. C. Schatz, *J. Phys. Chem. Lett.*, 2010, **1**, 1781-1788.
28. V. A. Ngo, R. K. Kalia, A. Nakano and P. Vashishta, *J. Phys. Chem. C*, 2012, **116**, 19579-19585.
29. G. Hu, B. Jiao, X. Shi, R. P. Valle, Q. Fan and Y. Y. Zuo, *ACS Nano*, 2013, **7**, 10525-10533.
30. O. Stueker, V. A. Ortega, G. G. Goss and M. Stepanova, *Small*, 2014, **10**, 2006-2021.
31. J. Lin, H. Zhang, Z. Chen and Y. Zheng, *ACS Nano*, 2010, **4**, 5421-5429.
32. J.-Q. Lin, H.-W. Zhang, Z. Chen, Y.-G. Zheng, Z.-Q. Zhang and H.-F. Ye, *J. Phys. Chem. C*, 2011, **115**, 18991-18998.
33. H.-M. Ding, W.-D. Tian and Y.-Q. Ma, *ACS Nano*, 2012, **6**, 1230-1238.
34. E. Heikkilä, H. Martinez-Seara, A. A. Gurtovenko, I. Vattulainen and J. Akola, *Biochim. Biophys. Acta, Biomembr.*, 2014, **1838**, 2852-2860.
35. J. F. Hainfeld and R. D. Powell, *J. Histochem. Cytochem.*, 2000, **48**, 471-480.
36. H. Jeon and G. G. Shipley, *J. Biol. Chem.*, 2000, **275**, 30458-30464.
37. H. Jeon and G. G. Shipley, *J. Biol. Chem.*, 2000, **275**, 30465-30470.
38. H. Margus, K. Padari and M. Pooga, *Adv. Drug Delivery Rev.*, 2013, **65**, 1031-1038.
39. M. W. Schmidt, K. K. Baldridge, J. A. Boatz, S. T. Elbert, M. S. Gordon, J. H. Jensen, S. Koseki, N. Matsunaga, K. A. Nguyen, S. Su, T. L. Windus, M. Dupuis and J. A. Montgomery, *J. Comput. Chem.*, 1993, **14**, 1347-1363.
40. P. J. Hay and W. R. Wadt, *J. Chem. Phys.*, 1985, **82**, 299-310.
41. B. H. Besler, K. M. Merz and P. A. Kollman, *J. Comput. Chem.*, 1990, **11**, 431-439.
42. Y. Duan, C. Wu, S. Chowdhury, M. C. Lee, G. Xiong, W. Zhang, R. Yang, P. Cieplak, R. Luo, T. Lee, J. Caldwell, J. Wang and P. Kollman, *J. Comput. Chem.*, 2003, **24**, 1999-2012.
43. W. L. Jorgensen, D. S. Maxwell and J. Tirado-Rives, *J. Am. Chem. Soc.*, 1996, **118**, 11225-11236.
44. P. r. Bjelkmar, P. Larsson, M. A. Cuendet, B. Hess and E. Lindahl, *J. Chem. Theory Comput.*, 2010, **6**, 459-466.
45. A. D. MacKerell, D. Bashford, Bellott, R. L. Dunbrack, J. D. Evanseck, M. J. Field, S. Fischer, J. Gao, H. Guo, S. Ha, D. Joseph-McCarthy, L. Kuchnir, K. Kuczera, F. T. K. Lau, C. Mattos, S. Michnick, T. Ngo, D. T. Nguyen, B. Prodhom, W. E. Reiher, B. Roux, M. Schlenkrich, J. C. Smith, R. Stote, J. Straub, M. Watanabe, J. Wiórkiewicz-Kuczera, D. Yin and M. Karplus, *J. Phys. Chem. B*, 1998, **102**, 3586-3616.
46. A. D. Mackerell, M. Feig and C. L. Brooks, *J. Comput. Chem.*, 2004, **25**, 1400-1415.
47. J. Huang and A. D. MacKerell, *J. Comput. Chem.*, 2013, **34**, 2135-2145.
48. C. Oostenbrink, A. Villa, A. E. Mark and W. F. Van Gunsteren, *J. Comput. Chem.*, 2004, **25**, 1656-1676.
49. W. L. Jorgensen, J. Chandrasekhar, J. D. Madura, R. W. Impey and M. L. Klein, *J. Chem. Phys.*, 1983, **79**, 926-935.
50. J. Hermans, H. J. C. Berendsen, W. F. Van Gunsteren and J. P. M. Postma, *Biopolymers*, 1984, **23**, 1513-1518.
51. J. L. F. Abascal and C. Vega, *J. Chem. Phys.*, 2005, **123**, 234505.
52. G. D. Hawkins, C. J. Cramer and D. G. Truhlar, *J. Phys. Chem.*, 1996, **100**, 19824-19839.
53. H. Heinz, R. A. Vaia, B. L. Farmer and R. R. Naik, *J. Phys. Chem. C*, 2008, **112**, 17281-17290.
54. D. Van Der Spoel, E. Lindahl, B. Hess, G. Groenhof, A. E. Mark and H. J. C. Berendsen, *J. Comput. Chem.*, 2005, **26**, 1701-1718.
55. G. Bussi, D. Donadio and M. Parrinello, *J. Chem. Phys.*, 2007, **126**, 014101-014107.
56. T. Darden, D. York and L. Pedersen, *J. Chem. Phys.*, 1993, **98**, 10089-10092.
57. B. Hess, H. Bekker, H. J. C. Berendsen and J. G. E. M. Fraaije, *J. Comput. Chem.*, 1997, **18**, 1463-1472.
58. B. Hess, *J. Chem. Theory Comput.*, 2008, **4**, 116-122.
59. W. Humphrey, A. Dalke and K. Schulten, *J. Mol. Graphics*, 1996, **14**, 33-38.
60. O. A. Andreev, A. G. Karabadzhak, D. Weerakkody, G. O. Andreev, D. M. Engelman and Y. K. Reshetnyak, *Proc. Natl. Acad. Sci. U.S.A.*, 2010, **107**, 4081-4086.
61. A. Kyrychenko, V. Vasquez-Montes, M. B. Ulmschneider and A. S. Ladokhin, *Biophys. J.*, 2015, **108**, 791-794.
62. P. Ferrara, J. Apostolakis and A. Caflisch, *Proteins: Structure, Function, and Bioinformatics*, 2002, **46**, 24-33.
63. R. Zhou, *Proteins: Structure, Function, and Bioinformatics*, 2003, **53**, 148-161.
64. H. Nguyen, J. Maier, H. Huang, V. Perrone and C. Simmerling, *J. Am. Chem. Soc.*, 2014, **136**, 13959-13962.
65. H. Nguyen, D. R. Roe and C. Simmerling, *J. Chem. Theory Comput.*, 2013, **9**, 2020-2034.
66. G. Nawrocki and M. Cieplak, *J. Phys. Chem. C*, 2014, **118**, 12929-12943.
67. S. Corni, M. Hnilova, C. Tamerler and M. Sarikaya, *J. Phys. Chem. C*, 2013, **117**, 16990-17003.
68. R. L. Willett, K. W. Baldwin, K. W. West and L. N. Pfeiffer, *Proc. Natl. Acad. Sci. U.S.A.*, 2005, **102**, 7817-7822.

69. O. Cohavi, D. Reichmann, R. Abramovich, A. B. Tesler, G. Bellapadrona, D. B. Kokh, R. C. Wade, A. Vaskevich, I. Rubinstein and G. Schreiber, *Chem. European J.*, 2011, **17**, 1327-1336.
70. B. R. Peelle, E. M. Krauland, K. D. Wittrup and A. M. Belcher, *Langmuir*, 2005, **21**, 6929-6933.
71. J. Yu, M. L. Becker and G. A. Carri, *Small*, 2010, **6**, 2242-2245.
72. Z. Tang, J. P. Palafox-Hernandez, W.-C. Law, Z. E. Hughes, M. T. Swihart, P. N. Prasad, M. R. Knecht and T. R. Walsh, *ACS Nano*, 2013, **7**, 9632-9646.
73. J. P. Palafox-Hernandez, Z. Tang, Z. E. Hughes, Y. Li, M. T. Swihart, P. N. Prasad, T. R. Walsh and M. R. Knecht, *Chem. Mater.*, 2014, **26**, 4960-4969.
74. L. M. Ghiringhelli, B. Hess, N. F. A. van der Vegt and L. Delle Site, *J. Am. Chem. Soc.*, 2008, **130**, 13460-13464.
75. C. Tamerler, M. Duman, E. E. Oren, M. Gungormus, X. Xiong, T. Kacar, B. A. Parviz and M. Sarikaya, *Small*, 2006, **2**, 1372-1378.
76. J. Feng, J. M. Slocik, M. Sarikaya, R. R. Naik, B. L. Farmer and H. Heinz, *Small*, 2012, **8**, 1049-1059.
77. R. Coppage, J. M. Slocik, B. D. Briggs, A. I. Frenkel, H. Heinz, R. R. Naik and M. R. Knecht, *J. Am. Chem. Soc.*, 2011, **133**, 12346-12349.
78. M. Hoefling, F. Iori, S. Corni and K.-E. Gottschalk, *Langmuir*, 2010, **26**, 8347-8351.
79. J. Yu, M. L. Becker and G. A. Carri, *Langmuir*, 2012, **28**, 1408-1417.
80. A. V. Verde, J. M. Acres and J. K. Maranas, *Biomacromolecules*, 2009, **10**, 2118-2128.
81. N. Almora-Barrios, G. Novell-Leruth, P. Whiting, L. M. Liz-Marzán and N. López, *Nano Lett.*, 2014, **14**, 871-875.
82. Y. K. Reshetnyak, O. A. Andreev, M. Segala, V. S. Markin and D. M. Engelman, *Proc. Natl. Acad. Sci. U.S.A.*, 2008, **105**, 15340-15345.
83. R. Sangram, C. Rahul, B. Susan, B. Julian, G. Zygmunt and G. Ignacy, *Methods Appl. Fluoresc.*, 2014, **2**, 035004.
84. X. Shi, D. Li, J. Xie, S. Wang, Z. Wu and H. Chen, *Chin. Sci. Bull.*, 2012, **57**, 1109-1115.
85. M. Hoefling, F. Iori, S. Corni and K.-E. Gottschalk, *ChemPhysChem*, 2010, **11**, 1763-1767.
86. P. L. Freddolino, C. B. Harrison, Y. Liu and K. Schulten, *Nat. Phys.*, 2010, **6**, 751-758.
87. P. Tian, *Annual Reports Section "C" (Physical Chemistry)*, 2008, **104**, 142-164.
88. F. Jiang, C.-Y. Zhou and Y.-D. Wu, *J. Phys. Chem. B*, 2014, **118**, 6983-6998.
89. F. Jiang and Y.-D. Wu, *J. Am. Chem. Soc.*, 2014, **136**, 9536-9539.
90. M. Paloncýová, G. Fabre, R. H. DeVane, P. Trouillas, K. Berka and M. Otyepka, *J. Chem. Theory Comput.*, 2014, **10**, 4143-4151.
91. J. Vymětal and J. Vondrášek, *J. Chem. Theory Comput.*, 2013, **9**, 441-451.
92. D. Petrov and B. Zagrovic, *PLoS Comput. Biol.*, 2014, **10**, e1003638.
93. S. Piana, J. L. Klepeis and D. E. Shaw, *Curr. Opin. Struct. Biol.*, 2014, **24**, 98-105.
94. E. C. Dreaden, M. A. Mackey, X. Huang, B. Kang and M. A. El-Sayed, *Chem. Soc. Rev.*, 2011, **40**, 3391-3404.
95. F. Iori, R. Di Felice, E. Molinari and S. Corni, *J. Comput. Chem.*, 2009, **30**, 1465-1476.
96. L. B. Wright, P. M. Rodger, S. Corni and T. R. Walsh, *J. Chem. Theory Comput.*, 2013, **9**, 1616-1630.
97. L. B. Wright, P. M. Rodger, T. R. Walsh and S. Corni, *J. Phys. Chem. C*, 2013, **117**, 24292-24306.